Model-Based Analysis of Myocardial Contraction Patterns in Ischemic Heart Disease

O. Duport, V. Le Rolle, E Galli, D. Danan, E. Darrigrand, E Donal, A.I. Hernández

Graphical abstract

IRBM ●●●●, ●●●, ●●●

Model-based analysis of myocardial contraction patterns in ischemic heart disease

O. Duport[a], V. Le Rolle[a,*], E. Galli[a], D. Danan[a], E. Darrigrand[b], E. Donal[a], A.I. Hernández[a]

[a] *Univ Rennes, CHU Rennes, Inserm, LTSI - UMR 1099, F-35000 Rennes, France*
[b] *Univ Rennes, IRMAR - UMR 6625, F-35000 Rennes, France*

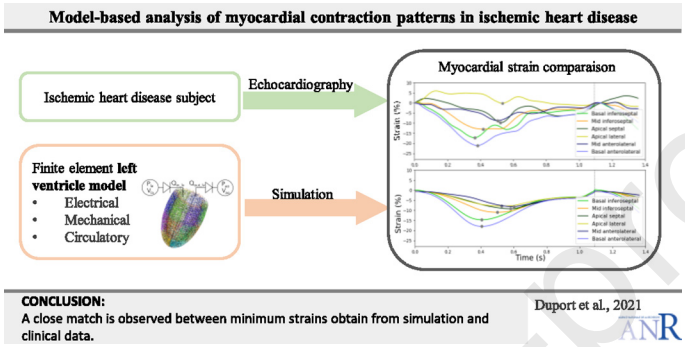

Highlights

- Left ventricle model including electro-mechanical activity and loading conditions.
- A coupling algorithm between the finite-element and lumped-parameter models.
- Simulation of hemodynamic variables and myocardial strains in ischemic heart disease.

Model-based analysis of myocardial contraction patterns in ischemic heart disease*

O. Duport[a], V. Le Rolle[a], E. Galli[a], D. Danan[a], E. Darrigrand[b], E. Donal[a] and A.I. Hernández[a]

[a] Univ Rennes, CHU Rennes, Inserm, LTSI - UMR 1099, F-35000 Rennes, France
[b] Univ Rennes, IRMAR - UMR 6625, F-35000 Rennes, France

ARTICLE INFO

Keywords:
Multi-physics modeling
Cardiac mechanics
Ischemic heart diseases
Experimental data

ABSTRACT

Objectives: The objective of the current study is to assess the feasibility of using a left ventricle (LV) model in order to reproduce myocardial strains in the case of ischemic heart disease (IHD).
Materials and Methods: The proposed integrated LV model couples a finite element method (FEM) sub-model of the cardiac electrical activity, representing the propagation of the trans-membrane potential through the LV, a FEM sub-model of the cardiac mechanical activity, and a lumped-parameter model of the circulatory system that improves the physiological definition of appropriate boundary conditions. Simulations were compared to myocardial strain data obtained from echocardiography, performed on two healthy subjects and two patients diagnosed with chronic IHD.
Results: Results show the model ability to simulate jointly the hemodynamic variables (Systolic and diastolic pressures respectively equal to 110 and 60 mmHg) and myocardial strain curves during each phase of the cardiac cycle. A close match is observed between minimum strains obtained from simulations and clinical data from healthy subjects and IHD patient, with a root mean square error around $2,81\%$ and $2,63\%$ respectively. The modifications of regional LV systolic strains observed from IHD patients with respect to healthy cases were partially explained by a decrease of regional cardiac stress.
Conclusion: This paper provides a description of a new coupling algorithm between FEM and lumped-parameter models. Results are promising for the analysis of cardiac strains in the context of IHD.

1. Introduction

Ischemic heart diseases (IHD), also known as coronary artery disease, usually occurs when coronary arteries, which supply heart with blood, oxygen and nutrients, become damaged or diseased. The imbalance between oxygen demand and supply results in an impairment of contractile function Henn, Cupps, Kar, Kulshrestha, Koerner, Braverman and Pasque (2015). Assessing the impact of IHD on the cardiac mechanical function may be performed by echocardiography, by evaluating regional myocardial kinetics and deformation (strain) Hoit (2011). These alterations of LV mechanics can be due to changes in contractility, loading conditions, and LV geometry Mada, Duchenne and Voigt (2014). However, echocardiography imaging could not be used to assess ventricular pressure or myocardial stress and is, thus, not able to take into account loading conditions. In this context, modeling of cardiac activity could be useful in order to provide a better understanding of myocardial deformations observed in IHD.

Modeling cardiac mechanics is a challenging task, mainly because of the lack of observability and the complexity of the mechanical properties of myocardial tissues. A variety of cardiac electro-mechanical modeling methods have been proposed in the literature, at many different levels of detail Niederer SA (2019). Most models are based on the Finite Element Method (FEM) to simulated time-varying cardiac mechanics Ponnaluri AVS (2019), Gsell (2018) Crozier, Blazevic, Lamata, Plank, Ginks, Duckett, Sohal, Shetty, Rinaldi, Razavi and et al. (2016) Constantino, Hu and Trayanova (2012). Simulations and personalization of these models usually require high computational resources. Some alternative solutions have been proposed to overcome this computational cost for the analysis of myocardial strains Walmsley, Huntjens, Prinzen, Delhaas and Lumens (2016) Lumens, Leenders, Cramer, De Boeck, Doevendans, Prinzen and Delhaas (2012) Everdingen, W.M.; Walmsley, Cramer, van Hagen, De Boeck, Meine, Delhaas, Doevendans, Prinzen and Lumens (2017). Our team has also proposed a patient-specific model-based analysis

* This document is the results of the research project funded by the French National Research Agency (ANR) (ANR-16-CE19-0008-01) (project MAESTRo).
*Corresponding author
ORCID(s): 0000-0003-1068-5587 (V. Le Rolle)

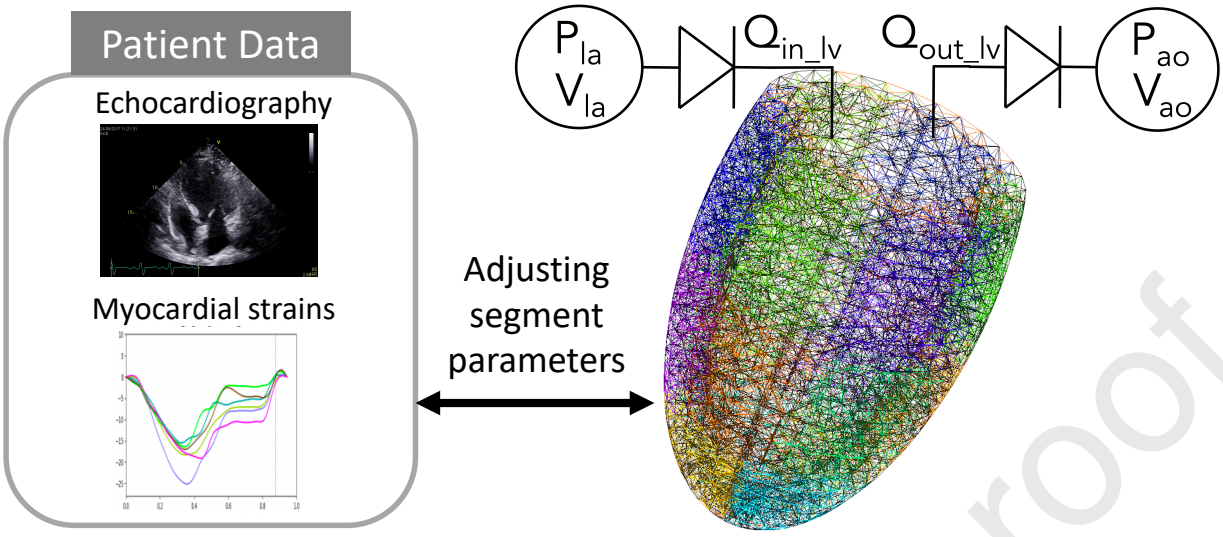

Figure 1: **Left panel**: Strain-derived curves obtained from each patient were compared to the outputs of the model and used to adjust the model's parameters. **Right panel**: Coupling between the lumped-parameter model of the circulation and the 3D model of the LV, which was divided in 16 segment according to the standardized segmentation of the AHA.

of myocardial strains Le Rolle, Hernandez, Richard, Donal and Carrault (2008), which has been recently adapted to analyse desynchronization strain patterns and contractility in left bundle branch block through computer model simulation Owashi, Taconne, Courtial, Simon, Garreau, Hernandez, Donal, Le Rolle and Galli (2022). However, these alternative approaches are based on simplified electromechanical laws and patient anatomy. As a consequence, some complementary approaches should be developed in order to propose tissue-level LV models that preserve computational costs, while integrating mechanical properties of myocardial tissues.

The aim of the current study was to assess the feasibility of using a relative low-resolution FEM LV model in order to evaluate regional contractility and to reproduce regional myocardial deformations in the case of IHD. One of the main challenge was to take into account loading conditions while preserving computational costs. The preload description should notably include the pulsatile behaviour of the left atria. Based on a preliminary version Le Rolle, Galli, Danan, El Houari, Hubert, Donal and Hernandez (2019), a 3D FEM model of LV electro-mechanical activity was proposed and coupled to a lumped-parameter model of preload and afterload. The document is organised as follows: in Section 2, the experimental data and an exhaustive description of the LV model, from the geometry to the multi-physics modelling and including the coupling procedures, are presented. Next in Section 3 and 4, the results of applying the described methods are presented and discussed.

2. Method

The proposed methodology is based on a model-based interpretation of LV contraction patterns observed in myocardial scarring. Two-dimensional transthoracic echocardiography was used to obtain deformation patterns in two healthy subjects and two patients with myocardial scar. A 3D FEM model of LV electro-mechanical activity was proposed and coupled to a lumped-parameter model of preload and afterload. Model parameters were evaluated manually to reproduce patient-derived strain curves obtained from echocardiography (figure 1).

2.1. Experimental data

2.1.1. Study Population

We prospectively included 2 healthy subjects and 2 patients, diagnosed with previous myocardial infarction and LV scar. We performed cardiac magnetic resonance imaging (cMRI) with late gadolinium enhancement (LGE) to localize myocardial scar when needed. The study was conducted according to the guidelines of the Declaration of Helsinki and approved by the local Institutional Ethics Committee.

2.1.2. Cardiac Magnetic Resonance Imaging

cMRI was performed using a 3-T clinical magnetic resonance system (Ingenia, Philips Medical Systems, Best, The Netherlands) with a 32-channel cardiovascular array coil. LGE images were acquired 10–15 min after intravenous administration of 0.2 mmol/kg of gadolinium (Gadoterate meglumine, Dotarem, Guerbet, Aulnay-sous-Bois, France), using 2D breath-hold inversion-recovery and phase-sensitive inversion-recovery sequences in the short-axis plane (spoiled gradient-echo, slice thickness 8 mm, repetition time 6.1 ms, echo time 2.9 ms, flip angle 25°, inversion time adjusted to null normal myocardium, typical breath-hold 11 s). The presence and localization of myocardial scar were assessed by a trained radiologist on a 16-segment LV model and the regional LGE extent was determined qualitatively and assessed on a per-segment basis.

2.1.3. Echocardiography

All patients underwent a standard TransThoracic Echocardiography (TTE) using a Vivid E9 ultrasound system (General Electric Healthcare, Horten, Norway). Images were recorded on a remote station for off-line analysis by dedicated software (EchoPAC PC, version BT 13, General Electric Healthcare, Horten, Norway) and segmental strain signals were obtained from standard apical 4-chamber, 3-chamber, and 2-chamber views.

2.2. Model of the left ventricle

2.2.1. Geometry

The left ventricle was approximated by a truncated ellipsoid Ω, whose parametrization in the undeformed configuration is given below

$$\mathbf{x} = \begin{pmatrix} x \\ y \\ z \end{pmatrix} = \begin{pmatrix} r_s \sin u \cos v \\ r_s \sin u \sin v \\ r_l \cos u \end{pmatrix} \tag{1}$$

The undeformed geometry is defined by the volume between:

- the endocardial surface Γ_{Endo}, $r_{si}, r_{li}, u \in [-\pi, -\arccos\frac{h}{r_{li}}], v \in [-\pi, \pi]$,
- the epicardial surface Γ_{Epi}, $r_{se}, r_{le}, u \in [-\pi, -\arccos\frac{h}{r_{le}}], v \in [-\pi, \pi]$,
- the base plane height h which is implicitly defined by the ranges for u.

Parameters r_{se}, r_{le} and h were evaluated specifically by fitting the truncated ellipsoid to the LV knot positions obtained from the semi-automatic segmentation of the endocardial wall, extracted from echocardiographic apical 4 and 2 chamber-views. Parameters r_{si}, r_{li} were computed by assuming the uniformity the left ventricular wall thickness. A 3D mesh was generated from this truncated ellipsoid by gmsh (`http://gmsh.info/`) Geuzaine and Remacle (2009). The mesh size is composed of about 10000 tetrahedrons with an average volume of 6 mm.

2.2.2. Electrical problem

The propagation of the transmembrane potential through the ventricle, under the equal anisotropy ratio assumption, was described as follows:

Problem $\mathcal{E}$. *Find a transmembrane potential* $V_m : \Omega \times [0,T] \to \mathbb{R}$ *and a ionic variable* $w : \Omega \times [0,T] \to \mathbb{R}$ *such that*

$$Div(\sigma_{eq} \nabla V_m) = \chi(C_m \frac{\partial V_m}{\partial t} + I_{ion}(V_m, w)) \qquad \text{in} \quad \Omega, \tag{2}$$

$$\frac{\partial w}{\partial t} = g(V_m, w) \qquad \text{in} \quad \Omega, \tag{3}$$

$$-(\sigma_{eq} \nabla V_m).\boldsymbol{\nu} = \begin{cases} I_{stim}(t) & \text{if } t < t_{exc} \\ 0 & \text{else} \end{cases} \qquad \text{on} \quad N_{exct}, \tag{4}$$

with $\sigma_{eq} = (\sigma_e^{-1} + \sigma_i^{-1})^{-1}$ *and, moreover,*

$$V_m(0) = V_m^0 \qquad \text{in} \quad \Omega, \tag{5}$$

$$w(0) = w^0 \qquad \text{in} \quad \Omega. \tag{6}$$

where $\sigma_e, \sigma_i, \sigma_{eq}$ are respectively the extracellular, intracellular and equivalent electrical conductivities, C_m is the membrane surface capacitance, χ is the rate of cellular membrane surface per volume unit and $\boldsymbol{\nu}$ is the unit outward normal vector. Here, (4) is a Neumann condition; a point N_{exct} of the domain Ω is electrically stimulated with a value I_{stim} for a preset time t_{exc}. The functions I_{ion} and g are described by the FitzHugh-Nagumo model Fitzhugh (1961):

$$I_{ion}(V_m, w) = kc_1(V_m - B)(a - \frac{V_m - B}{A})(1 - \frac{V_m - B}{A}) + kc_2 w(V_m - B) \tag{7}$$

$$g(V_m, w) = ke(\frac{V_m - B}{A} - dw - b). \tag{8}$$

where a, b, c_1, c_2, d, e, k, A and B are region specific parameters Sovilj S (2013); El Houari and Hernandez (2017). Problem $\mathcal{E}$ was solved with the finite element method (FEM) and the peak depolarization instants (T_s) were detected for each node during simulation.

2.2.3. Electrical-mechanical coupling

In order to represent, in a simplified manner, the complex processes involved in the electro-mechanical coupling at the tissue-level (e.g. calcium dynamics of each cell composing the tissue, effect of the heterogeneous mechanical activation of each cell, etc.), the choice was made in this work to represent the active constraint as an electro-mechanical activation function Le Rolle et al. (2008); Le Rolle, Carrault, Richard, Pibarot, Durand and Hernandez (2009). In order to take into account the asymmetry between the contraction and relaxation phases, a three-steps continuous Gaussian function was considered:

$$\sigma_a(t) = \begin{cases} \sigma_0 e^{-\psi_1 (t - T_m)^2} \text{ if } t \leq T_m \\ (\sigma_0 - \sigma_1) e^{-\psi_2 (t - T_m)^2} + \sigma_1 \text{ if } T_m < t \leq T_c \\ ((\sigma_0 - \sigma_1) e^{-\psi_2 (T_c - T_m)^2} + \sigma_1) e^{-\psi_3 (t - T_c)^2} \text{ otherwise} \end{cases} \tag{9}$$

where σ_0 is the amplitude of the active constraint signal, ψ_1 is a growth parameter associated to the contraction phase, ψ_2 and ψ_3 are growth parameters associated to the relaxation phase. T_m is the time of maximum active constraint, and T_c is the time of contraction of the left atrium.

2.2.4. Mechanical problem

Passive myocardial properties can be described through hyperelastic mechanical constitutive laws Land, Gurev, Arens, Augustin, Baron, Blake, Bradley, Castro, Crozier, Favino, Fastl, Fritz, Gao, Gizzi, Griffith, Hurtado, Krause, Luo, Nash, Pezzuto, Plank, Rossi, Ruprecht, Seemann, Smith, Sundnes, Rice, Trayanova, Wang, Jenny Wang and Niederer (2015). Although this kind of formulation allows a rather detailed description of the myocardium dynamics, it also requires higher computational resources Danan, Le Rolle, Hubert, Galli, Bernard, Donal, and Hernandez (2017). In this paper, linear elasticity was assumed in order to describe the ventricle motion:

Problem $\mathcal{M}$. *Find a displacement field* $\boldsymbol{u} : \Omega \times [0, T] \to \mathbb{R}^d$ *and a constraint field* $\boldsymbol{\sigma} : \Omega \times [0, T] \to \mathbb{M}^d$ *such that*

$$\boldsymbol{\sigma} = \boldsymbol{\sigma}_p + \sigma_a \boldsymbol{I} \qquad \text{in } \Omega \times [0, T], \tag{10}$$

$$\text{div}\, \boldsymbol{\sigma}(t) = \boldsymbol{0} \qquad \text{in } \Omega \times [0, T], \tag{11}$$

$$\boldsymbol{u}(t) = \boldsymbol{u}_{\Gamma_1} \qquad \text{on } \Gamma_{Basis} \times [0, T], \tag{12}$$

$$\boldsymbol{\sigma}(t)\boldsymbol{\nu} = \boldsymbol{p}(t) \qquad \text{on } \Gamma_{Endo} \times [0, T], \tag{13}$$

$$\boldsymbol{\sigma}(t)\boldsymbol{\nu} = 0 \qquad \text{on } \Gamma_{Epi} \times [0, T], \tag{14}$$

The Cauchy stress $\boldsymbol{\sigma}$ is composed of a passive component $\boldsymbol{\sigma}_p$ and an active component σ_a (9). Relation (11) is the equilibrium equation. The displacement in the base to the apex direction is set to zero, the circumferential motion in the basis endocardium is prevented (only radial motion is allowed), that is the so-called Dirichlet condition in (12), and the apex is free. Furthermore, the pressure is prescribed at the endocardium (13) and epicardium (14). Here, the passive material behaviour is modeled by a Hooke's law, meaning

$$(\sigma_p)_{ij} = \lambda\, \varepsilon_{kk} \delta_{ij} + 2\mu \varepsilon_{ij} \tag{15}$$

where we denote by λ and μ, the Lame coefficients, by δ_{ij} the Kronecker symbol and with

$$\varepsilon_{ij}(\boldsymbol{v}) = \frac{1}{2}\left(\frac{\partial v_i}{\partial x_j} + \frac{\partial v_j}{\partial x_i}\right) \tag{16}$$

and

$$\lambda = \frac{\kappa E}{(1+\kappa)(1-2\kappa)}, \qquad \mu = \frac{E}{2(1+\kappa)},$$

where $\boldsymbol{v}$ is the displacement vector, E the Young modulus, and κ the Poisson's ratio.

2.2.5. Circulatory model

The description of the volumes, pressures and flows through a cardiac cycle are given by a lumped-parameter model of the circulation. Left atria and ventricle were represented by elastance-based models, which offer a good compromise between complexity and number of parameters Smith, Andreassen, Shaw, Jensen, Rees and Chase (2007); Ugalde, Ojeda, Le Rolle, Andreu, Guiraud, Bonnet, Henry, Karam, Hagege, Mabo, Carrault and Hernandez (2016); Calvo, Le Rolle, Romero, Behar, Gomis, Mabo and Hernandez (2018a,b).

Problem $\mathcal{S}$. *Find the volume scalar fields V_{lv}, V_{la} and V_{ao} such that*

$$e_{la}(t) = e^{-B_{la}(t-C_{la}-t_{start_{la}})^2} \tag{17}$$
$$P_{la} = (e_{la}(t)(Ela_{max} - Ela_{min}) + Ela_{min})(V_{la} - V_{d_{la}}) \tag{18}$$
$$e_{lv}(t) = Ae^{-B_{lv}(t-C_{lv}-t_{start_{lv}})^2} \tag{19}$$
$$P_{lv} = e_{lv}(t)E_{lv}(V_{lv} - V_{d_{lv}}) + (1 - e_{lv}(t))P_{0_{lv}}(e^{\lambda_{lv}(V_{lv}-V_{0_{lv}})} - 1) \tag{20}$$
$$P_{ao} = V_{ao}/C_{ao} \tag{21}$$
$$Q_{R_{ao}} = P_{ao}/R_{ao} \tag{22}$$
$$Q_{in\_lv} = \begin{cases} (P_{la} - P_{lv})/R_{in\_lv} \text{ if } P_{lv} < P_{la} \\ 0 \text{ else.} \end{cases} \tag{23}$$
$$Q_{out\_lv} = \begin{cases} (P_{lv} - P_{ao})/R_{out\_lv} \text{ if } P_{lv} > P_{ao} \\ 0 \text{ else.} \end{cases} \tag{24}$$
$$Q_{R_{la}} = (P_{in0_{lv}} - P_{la})/R_{la} \tag{25}$$
$$\dot{V}_{lv} = Q_{in\_lv} - Q_{out\_lv} \tag{26}$$
$$\dot{V}_{la} = Q_{R_{la}} - Q_{in_{lv}} \tag{27}$$
$$\dot{V}_{ao} = Q_{out\_lv} - Q_{R_{ao}} \tag{28}$$

where P, V and Q are associated with pressure, volume and flux cavities, whereas subscribes ao, la and lv respectively stand for aorta, left atria and ventricle. Mitral and aortic valves are represented as diodes, which simulate the one-way direction of blood. Afterload pressure was calculated as a linear relationship between volume and vascular compliance C_{ao} (21) and flows between chambers was obtained by considering vascular resistance R_{ao} (22). $e_{la}(t)$ and $e_{lv}(t)$ are driver functions that controls time-variant elastance Ojeda, Rolle, Koon, Thebault, Donal and Hernández (2013); Calvo et al. (2018a). To account for the mechanical function of the atria, the atrial pressure P_{la} is represented as a linear function of its instantaneous volume V_{la}, whose slope E_{la} represents the elastic properties of the atrial wall (18). Regarding the left ventricle, its pressure is represented by a combination of the end-systolic and end-diastolic pressure-volume relationships (20), associated with parameters E_{lv}, $V_{d_{lv}}$, $P_{0_{lv}}$, λ_{lv}, $V_{0_{lv}}$.

2.2.6. Coupling procedure between circulation and the mechanical problem

In order to take into account the influence of loading conditions on myocardial strains, the electro-mechanical problem should be coupled to the circulatory model. Although some couplings have been already used to associate 3D cardiac model to lumped-parameter models of the circulation Bovendeerd, Borsje, Arts and van De Vosse (2006), the coupling algorithm is rarely described precisely. Briefly, it consists in estimating the volume predicted by the circulatory and electromechanical models through the left ventricular pressure, as long as the difference between these

volumes is not less than a predefined accuracy (Fig. 2). The index n stand for the time step in a numerical simulation, i the index of the step of the pressure-generating algorithm presented in this section (initialized at 0), FE refers to the electromechanical coupled problem solved with the finite element method and S refers to the hemodynamic problem derived from Problem S.

- **Step 1: Estimation of the left ventricular pressure**
  At the beginning of each time step, each first estimate of ventricular pressure is based on a fourth order Adams-Bashfort explicit scheme Kreyszig (2010); it uses previous pressures to extrapolate and estimate the new initial pressure

$$p^0_{lv,n+1} = f(p_{lv,n}, p_{lv,n-1}, p_{lv,n-2}, p_{lv,n-3}); \tag{29}$$

  except at the very first time step, where an initial value is considered.

- **Step 2: Volume estimation with the finite element model**
  The pressure $p^i_{lv,n+1}$ is applied to the endocardium surface, just as described in equation (13), and a new volume $V^i_{lv,FE}$ for the left ventricle is returned by solving the resulting electromechanical problem.

- **Step 3: Volume estimation based on the flows arising from the pressure**
  Volumes (26)-(28) and flows (22)-(25) are calculated using a mid-point scheme. Then, P_{la} and P_{ao} are updated with (18) and (21), respectively along with $V^i_{lv,S} = V^i_{lv,n+1}$.

- *Step*4**: Volumes comparison and next estimation**
  We compute the relative difference $\delta = \frac{|V^i_{lv,S} - V^i_{lv,FE}|}{V^i_{lv,S}}$ between these two volumes

  – If the criteria $\delta < \epsilon$ is satisfied, where ϵ is an arbitrarily small parameter, hemodynamic coupling is achieved.

  – Else, a next estimation of pressure $P^{i+1}_{lv,n+1}$ is calculated using a conjugate gradient method and we go back to Step 2.

The proposed algorithm allows the integration of electro-mechanical problem and the circulatory model. Cardiac valves states are determined by hemodynamic model and each cardiac cycle phase depends on the coupling between the two models.

2.3. Extraction of myocardial strains

In order to perform comparisons between simulations and clinical data, left ventricle was divided into 16 segment according to the standardized segmentation of the AHA Cerqueira, Weissman, Dilsizian, Jacobs, Kaul, Laskey, Pennell, Rumberger, Ryan and Verani (2002). The left ventricle is divided into equal thirds perpendicular to the long axis of the heart: *basal*, *mid-cavity*, and *apical*:

- Six segments of 60° each are used for the basal slice: *BasAnt*, *BasAntSept*, *BasInfSept*, *BasInf*, *BasInfLat*, and *BasAntLat*.
- The mid part is also divided into six 60° segments: *MidAnt*, *MidAntSept*, *MidInfSept*, *MidInf*, *MidInfLat*, and *MidAntLat*.
- Four segments of 90° each are used for the apex: *ApiAnt*, *ApiSept*, *ApiInf*, and *ApiLat*.

16 couples of points were considered, each of them belonging to a different segment *seg* of the left ventricle (Fig. 1). Let $x_{seg,1}(t)$, $x_{seg,2}(t)$ be the position of 2 points of interest at a given time t and let $X_{seg,1}$, $X_{seg,2}$ be the position of the same points in the reference configuration, then the strain $S(t)$ is defined by

$$S(t) = \Big(\frac{\|x_{seg,1}(t) - x_{seg,2}(t)\|}{\|X_{seg,1} - X_{seg,2}\|} - 1 \Big) \times 100 \tag{30}$$

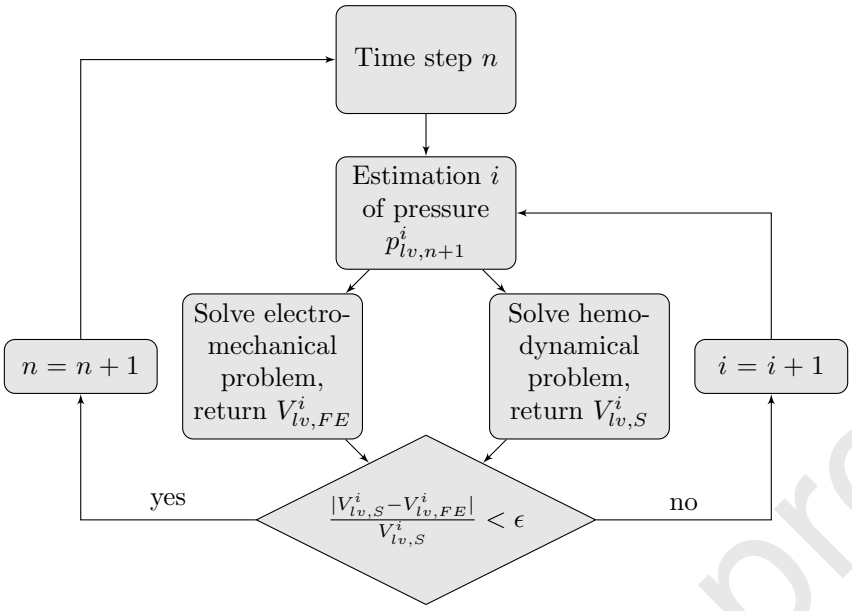

Figure 2: Pressure-generating algorithm used to obtain hemodynamic coupling

Reference configuration corresponds to the instant when the LV enters depolarization, during the first cycle of the fully coupled numerical simulation, at the end of the diastole. In this work, the parameter estimation was performed manually by varying the mechanical parameters in order to obtained simulated systolic and diastolic strain values similar to the observed clinical data. The different physical problems and numerical methods have been implemented in a code which is based on a finite element library in C++ under the GNU Public license: GEneric Tools for Finite Elements Methods (GETFEM++) (`https://savannah.nongnu.org/projects/getfem`).

3. Results

3.1. Hemodynamic simulations and myocardial strains in a healthy case

Fig. 3 presents the simulation of hemodynamic variables: ventricular pressure and volume for a cardiac cycle in healthy case. The systolic LV pressure is equal to 110 mmHg, and the aortic pressure varies between 60 and 105 mmHg. Ventricular volume is equal to 95 ml at the end of diastole and 45 ml at the end of diastole. For each cardiac cycle, myocardial strains were simulated jointly to hemodynamic variables. Pressure-volume loop illustrate the model ability to reproduce the four basic phases of the cardiac cycle: i) the isovolumic contraction phase; ii) the systole; iii) the isovolumic relaxation; iv) the diastole.

3.2. Analysis of myocardial strains

Figure 4 shows strain curves obtained at each location of the standardised AHA segmentation for two healthy subjects. The strain morphology corresponds globally to the clinical data. In fact, root mean square error (RMSE), calculated at minimum strain value, are respectively equal to 3.56% and 2.06% for the first and second subjects. During systole, strain values decrease with a negative peak around the aortic valve closure, representing the maximal longitudinal myocardial shortening during contraction. In diastole, strain values increase towards zero, which mean that the length of the analysed myocardial segment returns to its original length at the beginning of the cardiac cycle. The diastole period can be divided into three periods: the first one corresponding to a rapid filling phase due to an aspiration of blood inside the ventricle, a slower filling period and the late diastolic filling phase, corresponding to the atrial systole. Bull-eye plots, which are accepted analysis tools in cardiac diagnosis, were generated to depict minimum strains associated with each AHA segment. Bull-eyes on figure 4 show a close match between the minimum values of strains obtained from the simulated and experimental data.

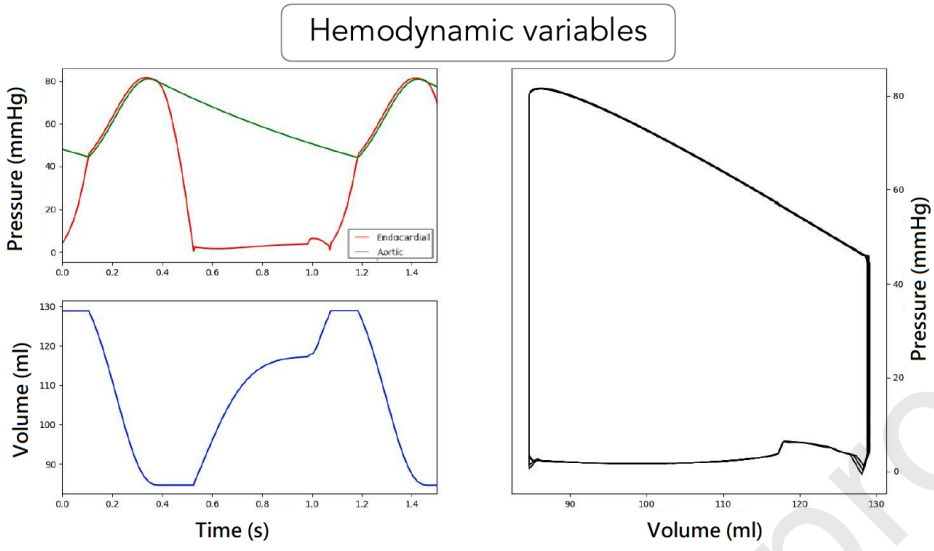

Figure 3: Aortic/endocardial pressure and endocardial volume through a cardiac cycle

Figure 5 illustrates simulated and experimental strains within scarred segments on the anterior (first column) and inferior (second column) walls. Since the shade is directly scaled with respect to the minimal value of the strain for the associated segment, bull-eye plots show some extent closeness between the simulation and the data. The RMSE calculated at minimum strain value was respectively equal to 2.41% and 2.84% for the anterior IHD and the inferior IHD subjects. Concerning the anterior ischemia case, a global increase of minimum strain values was observed for the anterior region, with maximum values equal to -5.8% and -6.2% for the *MidAnt* simulated and data strain. Similar increases of minimum strain values were observed for the inferior ischemia, which reach -6.5% and -3.4% for the *BasInf* segment.

Bull-eyes of figure 6 illustrate the maximum myocardial stresses associated with 2 healthy subjects and 2 chronic IHD patients. The two healthy cases show homogeneous stress values, whereas IHD patients presents low stress values on segments with diagnosed LV scar. On the anterior ischemia case, the global increase of minimum strain of the anterior region is associated with a decrease of maximum stress values for the concerned segments. Similarly, concerning the inferior IHD, minimum strains of inferior regions (especially *BasInf* and *BasInfLat*) increase in association with a diminution of stress values.

4. Discussion

In this paper, a model-based approach was proposed in order to analyse LV contraction patterns observed by echocardiography and to replicate the intrinsic electromechanical properties of the myocardium observed in two healthy subjects and two real-life patients with previous myocardial infarction (chronic IHD). The proposed model was able to reproduce local alteration that corresponds to the areas of myocardial scar observed with cMRI.

4.1. Model-based approach

Simulated strains illustrated the model ability to simulate jointly the hemodynamic variables and myocardial deformations. Strain curves notably reflected typical characteristics associated with each phase of the cardiac cycle. The LV model was also used to reproduce regional myocardial deformations in the case of IHD. We have observed a close match between minimum strains obtained from simulations and clinical data from chronic IHD patients. Our results show that the overall dynamics of strain curves in the LV scarred region could be partially explained by the regional decrease in cardiac stress. The proposed model-based approach thus provide a better understanding of strain curves observed with ischemic myocardial abnormalities.

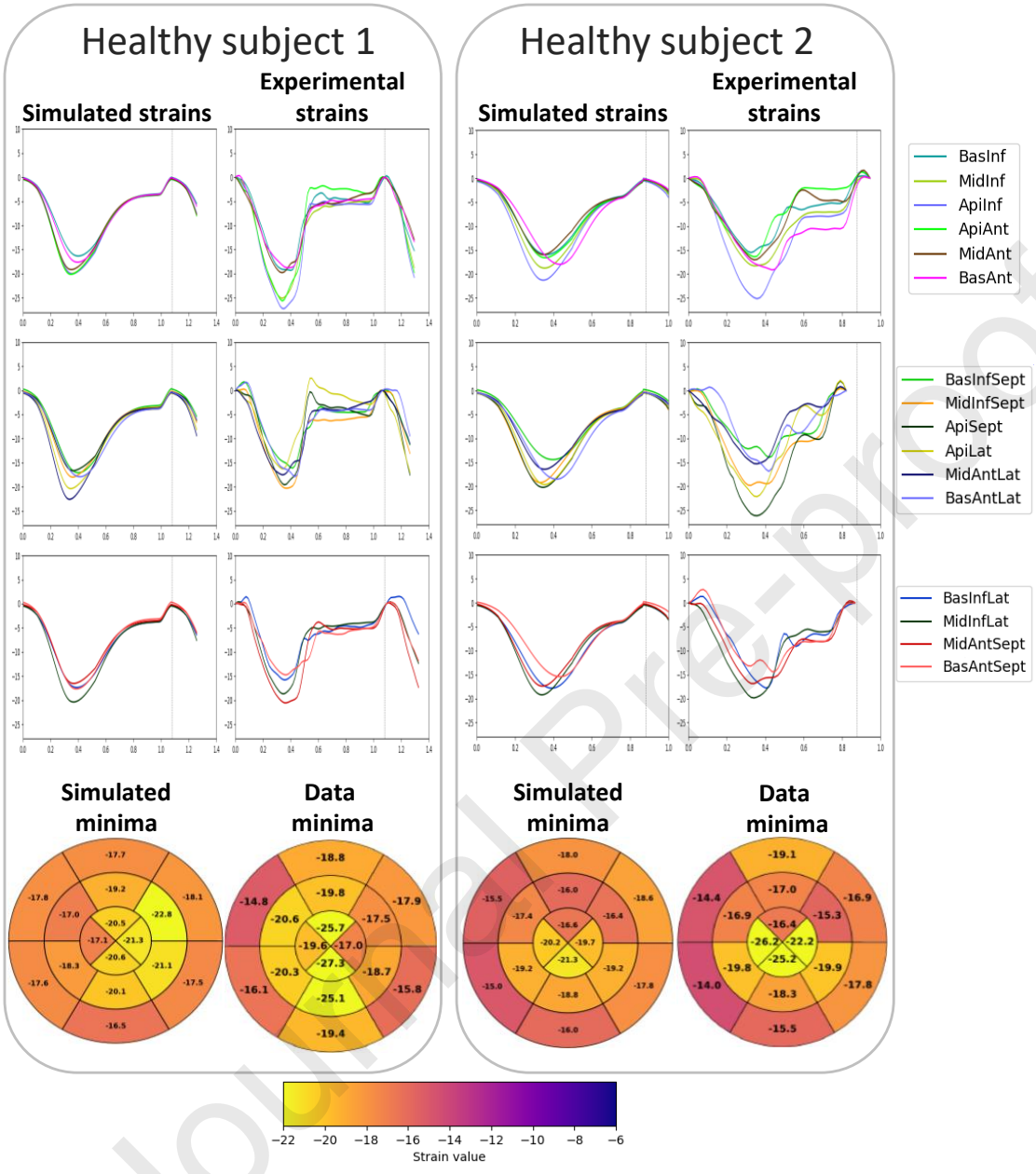

Figure 4: Comparison between simulated and experimental strain signals for 2 healthy cases (Upper panel). Minimum simulated and experimental strains in % (Bottom panel)

Although previous models (Albatat, Bergsland, Arevalo, Odland, Wall, Sundnes and Balasingham (2020)Connolly and Bishop (2016)) already proposed computational representations of myocardial infarct scars, our approach provides interesting points. Our approach requires low computational resources due to the level of detail of the model, which is consistent with a translation to clinical practice. In fact, the electrical model is based on the adapted monodomain formalism together with the FitzHugh-Nagumo representation and the mechanical part is represented by a simplified linear law. Although the model was defined from simplified assumptions, this approach has been already used in (Sovilj S (2013), Dokos, Cloherty and Lovell (2007), Kunisch and Souza (2018)) and have showed significant reduction

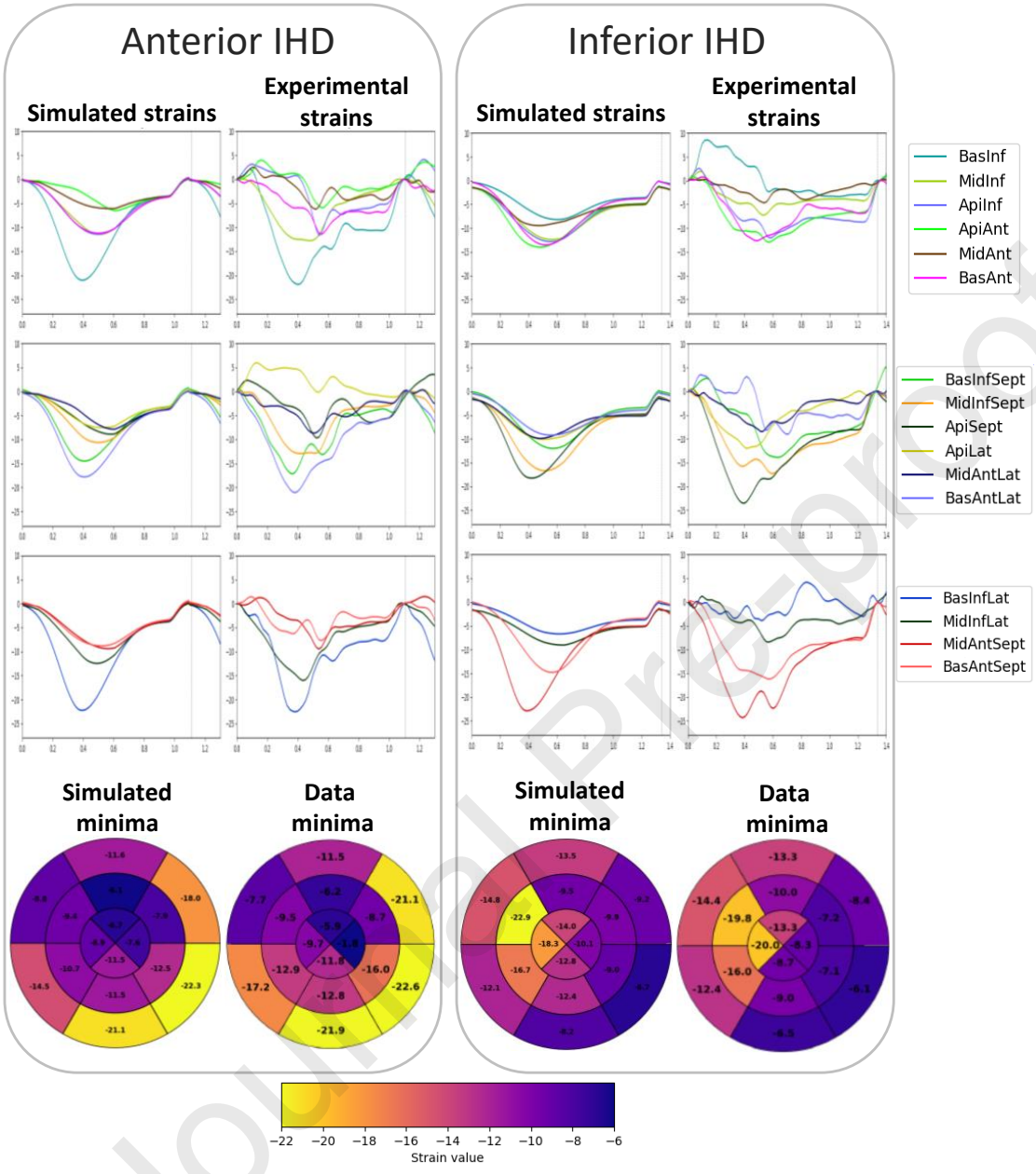

Figure 5: Comparison between simulated and experimental strain signals for inferior and anterior IHD patients (Upper panel). Minimum simulated and experimental strains in % (Bottom panel)

of: (i) the computational costs and (ii) the number of parameters that need to be tuned. One major contribution of this paper is the description of the coupling algorithm between a 3D model of LV and a lumped-parameter of the circulation. This coupling is essential to take into account preload and afterload influence on patterns of LV contraction. The results, illustrating similarities between simulations and clinical data, show potential applications in personalized therapy and the global approach is an important step toward the proposition of personalized models since it allows low computational costs and realistic boundary conditions.

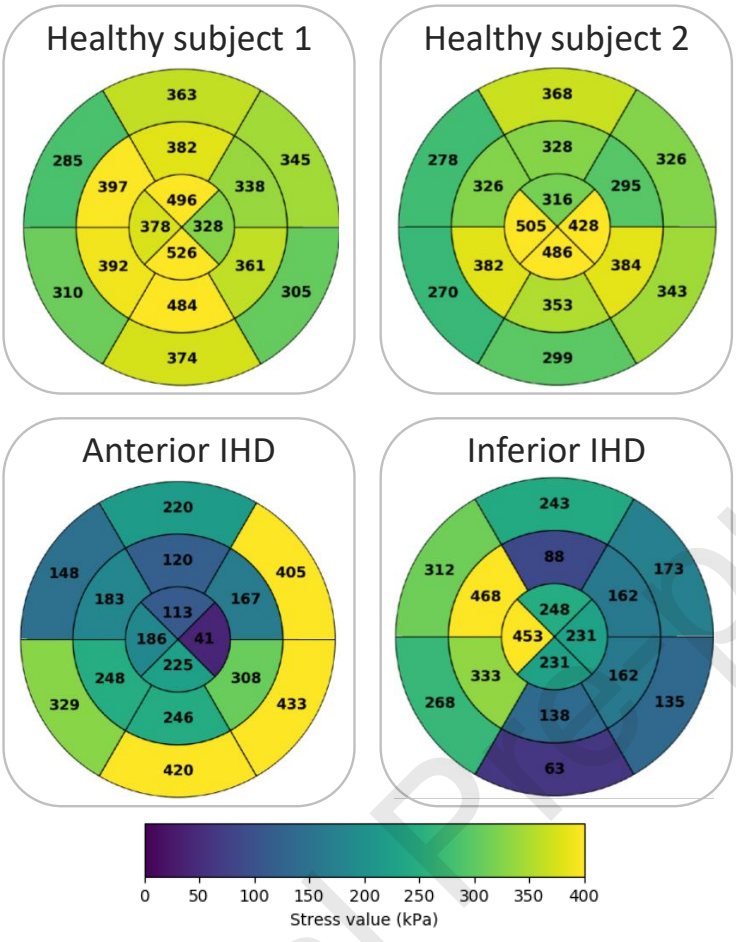

Figure 6: Bull-eye of maximum stress values in kPa (A)

4.2. Strain Patterns and Scar Localization

In IHD, modifications of myocardial strains are mainly characterized by *i)* regional inhomogeneities, *ii)* reduction of systolic strain within the ischemic segments, and *iii)* alteration in the onset and duration of fibre contraction, which leads to a characteristic shortening or thickening of the myocardium after aortic valve closure Mada et al. (2014). Reduction in systolic strain is related to significant modifications of regional cardiac function. IHD is usually caused by a reduction of blood flow in the coronary vessels, which results in a lack of oxygen consumption and a decrease of force production Allen and Orchard (1987). The regional differences of myocardial contractility also induce some regional inhomogeneities of cardiac strains Mada et al. (2014). In fact, all segments that are associated with reduced contractility do not bring an effective contribution to blood ejection and could affect the contraction of neighboring segments. In clinical practice, the area of reduced contractility in ischemic patients is usually assessed visually, which might lead to poor reproducibility because the visual identification of these contraction patterns is largely influenced by the experience of the clinician. The proposed computational model was able to disclose the characteristics of the LV deformation patterns observed in patients of both ischemic and non-ischemic etiology. In fact, results show that segments with increased systolic strains are associated with important reductions in myocardial stress, which reflect the alteration of cardiac function due to local scar Lee and Allen (1991).

4.3. Limitations

Nevertheless, some limitations should be mentioned. First, the strain curve dynamics is not completely reproduced with the LV model. Previous work have shown that the strain curves obtained in ischemic segments are characterized

by a reduced strain peak, which occurs after the aortic valve closure Voigt, Exner, Schmiedehausen, Huchzermeyer, Reulbach, Nixdorff, Platsch, Kuwert, Daniel and Flachskampf (2003). This morphology, also referred as "post-systolic shortening" is only partially explained by the regional decrease in cardiac stress. The reciprocal interaction between neighbour segments, between LV scarred segments and normal LV segments, as far as sub-clinical LV conduction disturbances and changes in the overall LV geometry, might contribute to the typical strain pattern observed in IHD Voigt et al. (2003); Asanuma and Nakatani (2015). Improvements concerning the electro-mechanical function will be proposed and the possibility of integrating a hyper-elastic law will be analyzed as in previous work of our team Danan et al. (2017). In futur works, the right ventricle will be included in order to improve simulations of strain morphologies. Some limitations are also related to the manual adjustment of model parameters. In future developments, identification algorithms will be implemented to reduce the error between simulated and experimental strains, as done in our previous works Le Rolle et al. (2008, 2009). Finally, this study is based on a small population of IHD patients leading to moderately significant results and, thus, conclusions should be extracted by means of a larger clinical series.

5. Conclusion

The objective of this study was to propose a model-based interpretation of the different patterns of LV contraction observed in the case of preserved contractility and myocardial scarring. A mathematical model of the left ventricle, including the coupling between the 3D description of electro-mechanical activity and the influence of circulation, was proposed and analyzed. One contribution of this work is the description of the coupling algorithm between the FEM and lumped-parameter models. The integration algorithm is essential to describe both cardiac electrical, mechanical, and hemodynamic influence on LV contraction patterns. The integrated model reproduced the reduction of minimum strains observed in myocardial ischemia. The ischemic segments presented reduced contractility, as expressed by the smaller active parameters. The results are promising for the analysis of cardiac strains in the context of IHD and provide novel insights into the complex deformations of the left ventricle.

CRediT authorship contribution statement

O. Duport: Formal analysis, Data curation, Methodology, Software, Writing - review & editing. **V. Le Rolle:** Conceptualization, Funding acquisition, Data curation, formal analysis, Methodology, Software, Supervision, Writing - Original draft, Writing - review & editing. **E. Galli:** Data curation, Supervision, Writing - review & editing. **D. Danan:** formal analysis, Methodology, Software, Writing - review & editing. **E. Darrigrand:** Formal analysis, Methodology, Writing - review & editing. **E. Donal:** Data curation, Writing - Original draft preparation, Supervision, Writing - review & editing. **A.I. Hernández:** Conceptualization, Data curation, formal analysis, Methodology, Software, Writing - original draft, Supervision, Writing - review & editing.

References

Albatat, M., Bergsland, J., Arevalo, H., Odland, H., Wall, S., Sundnes, J., Balasingham, I., 2020. Multisite pacing and myocardial scars: a computational study. Comput Methods Biomech Biomed Engin 23, 248–260.

Allen, D.G., Orchard, C.H., 1987. Myocardial contractile function during ischemia and hypoxia. Circ. Res. 60, 153–168.

Asanuma, T., Nakatani, S., 2015. Myocardial ischaemia and post-systolic shortening. Heart 101, 509–516.

Bovendeerd, P.H., Borsje, P., Arts, T., van De Vosse, F.N., 2006. Dependence of intramyocardial pressure and coronary flow on ventricular loading and contractility: a model study. Ann Biomed Eng 34, 1833–1845.

Calvo, M., Le Rolle, V., Romero, D., Behar, N., Gomis, P., Mabo, P., Hernandez, A.I., 2018a. Model-based analysis of the autonomic response to head-up tilt testing in Brugada syndrome. Comput. Biol. Med. 103, 82–92.

Calvo, M., Le Rolle, V., Romero, D., Behar, N., Gomis, P., Mabo, P., Hernandez, A.I., 2018b. Recursive model identification for the analysis of the autonomic response to exercise testing in Brugada syndrome. Artif Intell Med .

Cerqueira, M.D., Weissman, N.J., Dilsizian, V., Jacobs, A.K., Kaul, S., Laskey, W.K., Pennell, D.J., Rumberger, J.A., Ryan, T., Verani, M.S., 2002. Standardized myocardial segmentation and nomenclature for tomographic imaging of the heart. A statement for healthcare professionals from the Cardiac Imaging Committee of the Council on Clinical Cardiology of the American Heart Association. Int J Cardiovasc Imaging 18, 539–542.

Connolly, A., Bishop, M., 2016. Computational representations of myocardial infarct scars and implications for arrhythmogenesis. Clin Med Insights Cardiol 10, 27–40.

Constantino, J., Hu, Y., Trayanova, N., 2012. A computational approach to understanding the cardiac electromechanical activation sequence in the normal and failing heart, with translation to the clinical practice of crt. Prog. Biophys. Mol. Biol. 110, 372–379.

Crozier, A., Blazevic, B., Lamata, P., Plank, G., Ginks, M., Duckett, S., Sohal, M., Shetty, A., Rinaldi, C., Razavi, R., et al., 2016. The relative role of patient physiology and device optimisation in cardiac resynchronisation therapy: A computational modelling study. J. Mol. Cell. Cardiol. 96, 93–100.

Danan, D., Le Rolle, V., Hubert, A., Galli, E., Bernard, A., Donal, E., , Hernandez, A., 2017. Validation of a Finite Element Method framework for cardiac mechanics applications. 13th International Symposium on Medical Information Processing and Analysis .

Dokos, S., Cloherty, S., Lovell, N., 2007. Computational model of atrial electrical activation and propagation. 29th annual international conference of the IEEE engineering in medicine and biology society , 908–911.

El Houari, K., K.A.A.L.B.S.K.A.B.G.C.R.M., Hernandez, A., 2017. A fast model for solving the ECG forward problem based on an evolutionary algorithm. Computational Advances in Multi-Sensor Adaptive Processing (CAMSAP) , IEEE 7th International Workshop on (2017), IEEE, pp. 15.

Everdingen, V., W.M.; Walmsley, J., Cramer, M., van Hagen, I., De Boeck, B., Meine, M., Delhaas, T., Doevendans, P., Prinzen, F., Lumens, J.e.a., 2017. Echocardiographic prediction of cardiac resynchronization therapy response requires analysis of both mechanical dyssynchrony and right ventricular function: A combined analysis of patient data and computer simulations. J. Am. Soc. Echocardiogr. 30, 1012–1020.

Fitzhugh, R., 1961. Impulses and Physiological States in Theoretical Models of Nerve Membrane. Biophys. J. 1, 445–466.

Geuzaine, C., Remacle, J.F., 2009. Gmsh: a three-dimensional finite element mesh generator with built-in pre- and post-processing facilities. International Journal for Numerical Methods in Engineering , 1309–1331.

Gsell, M., A.C.M.P.A.J.K.E.F.J.F.K.M.G.L.K.T..P.G., 2018. Assessment of wall stresses and mechanical heart power in the left ventricle: Finite element modeling versus Laplace analysis. International journal for numerical methods in biomedical engineering , 34(12).

Henn, M.C., Cupps, B.P., Kar, J., Kulshrestha, K., Koerner, D., Braverman, A.C., Pasque, M.K., 2015. Quantifying "normalized" regional left ventricular contractile function in ischemic coronary artery disease. J. Thorac. Cardiovasc. Surg. 150, 240–246.

Hoit, B.D., 2011. Strain and strain rate echocardiography and coronary artery disease. Circ Cardiovasc Imaging 4, 179–190.

Kreyszig, E., 2010. Advanced Engineering Mathematics. Wiley & Sons, New York, 10th Edition , 911–912.

Kunisch, K., Souza, D., 2018. On the one-dimensional nonlinear monodomain equations with moving controls. J de Mathematiques Pures et Appliquees 117, 94–122.

Land, S., Gurev, V., Arens, S., Augustin, C.M., Baron, L., Blake, R., Bradley, C., Castro, S., Crozier, A., Favino, M., Fastl, T.E., Fritz, T., Gao, H., Gizzi, A., Griffith, B.E., Hurtado, D.E., Krause, R., Luo, X., Nash, M.P., Pezzuto, S., Plank, G., Rossi, S., Ruprecht, D., Seemann, G., Smith, N.P., Sundnes, J., Rice, J.J., Trayanova, N., Wang, D., Jenny Wang, Z., Niederer, S.A., 2015. Verification of cardiac mechanics software: benchmark problems and solutions for testing active and passive material behaviour. Proc. Math. Phys. Eng. Sci. 471, 20150641.

Le Rolle, V., Carrault, G., Richard, P.Y., Pibarot, P., Durand, L.G., Hernandez, A.I., 2009. A tissue-level electromechanical model of the left ventricle: application to the analysis of intraventricular pressure. Acta Biotheor. 57, 457–478.

Le Rolle, V., Galli, E., Danan, D., El Houari, K., Hubert, A., Donal, E., Hernandez, A.I., 2019. Sensitivity Analysis of a Left Ventricle Model in the Context of Intraventricular Dyssynchrony. Acta Biotheor. .

Le Rolle, V., Hernandez, A.I., Richard, P.Y., Donal, E., Carrault, G., 2008. Model-based analysis of myocardial strain data acquired by tissue Doppler imaging. Artif Intell Med 44, 201–219.

Lee, J.A., Allen, D.G., 1991. Mechanisms of acute ischemic contractile failure of the heart. Role of intracellular calcium. J. Clin. Invest. 88, 361–367.

Lumens, J., Leenders, G., Cramer, M., De Boeck, B., Doevendans, P., Prinzen, F., Delhaas, T., 2012. Mechanistic evaluation of echocardiographic dyssynchrony indices patient data combined with multiscale computer simulations. Circ. Cardiovasc. Imaging 5, 491–499.

Mada, R.O., Duchenne, J., Voigt, J.U., 2014. Tissue Doppler, strain and strain rate in ischemic heart disease how I do it. Cardiovasc Ultrasound 12, 38.

Niederer SA, Lumens J, T.N., 2019. Computational models in cardiology. Nat Rev Cardiol. , 16(2):100–111.

Ojeda, D., Rolle, V.L., Koon, K.T.V., Thebault, C., Donal, E., Hernández, A.I., 2013. Towards an atrio-ventricular delay optimization assessed by a computer model for cardiac resynchronization therapy, in: Proc. SPIE 8922, IX International Seminar on Medical Information Processing and Analysis.

Owashi, K., Taconne, M., Courtial, N., Simon, A., Garreau, M., Hernandez, A., Donal, E., Le Rolle, V., Galli, E., 2022. Desynchronization strain patterns and contractility in left bundle branch block through computer model simulation. J. Cardiovasc. Dev. Dis. 9, 53.

Ponnaluri AVS, Verzhbinsky IA, E.J.G.A.E.D.P.L., 2019. Model of Left Ventricular Contraction: Validation Criteria and Boundary Conditions. Funct Imaging Model Heart. , 11504:294–303.

Smith, B.W., Andreassen, S., Shaw, G.M., Jensen, P.L., Rees, S.E., Chase, J.G., 2007. Simulation of cardiovascular system diseases by including the autonomic nervous system into a minimal model. Comput Methods Programs Biomed 86, 153–160.

Sovilj S, Magjarevic, L.N.D.S., 2013. A simplified 3D model of whole heart electrical activity and 12-lead ECG generation. Comput Math Methods Med. , 2013:134208.

Ugalde, H.M., Ojeda, D., Le Rolle, V., Andreu, D., Guiraud, D., Bonnet, J.L., Henry, C., Karam, N., Hagege, A., Mabo, P., Carrault, G., Hernandez, A.I., 2016. Model-Based Design and Experimental Validation of Control Modules for Neuromodulation Devices. IEEE Trans Biomed Eng 63, 1551–1558.

Voigt, J.U., Exner, B., Schmiedehausen, K., Huchzermeyer, C., Reulbach, U., Nixdorff, U., Platsch, G., Kuwert, T., Daniel, W.G., Flachskampf, F.A., 2003. Strain-rate imaging during dobutamine stress echocardiography provides objective evidence of inducible ischemia. Circulation 107, 2120–2126.

Walmsley, J., Huntjens, P.R., Prinzen, F.W., Delhaas, T., Lumens, J., 2016. Septal flash and septal rebound stretch have different underlying mechanisms. Am. J. Physiol. Heart Circ. Physiol. 310, 394–403.

Graphical Abstract

Model-based analysis of myocardial contraction patterns in ischemic heart disease

O. Duport,V. Le Rolle,E. Galli,D. Danan,E. Darrigrand,E. Donal,A.I. Hernández

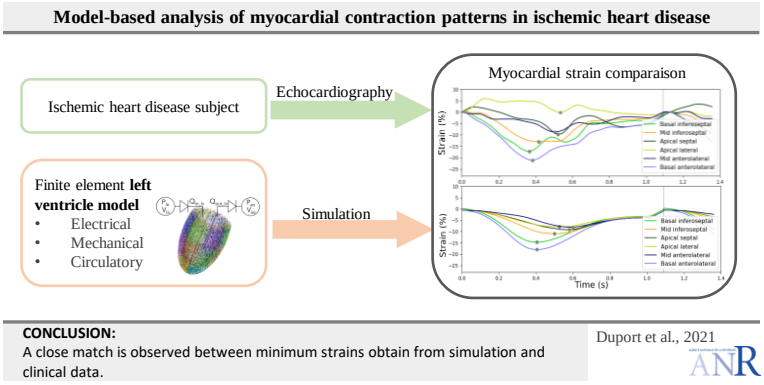

Author responsibilities, integrity, ethics

This is an **editable** PDF form. It should **be saved to your computer, then completed** using Adobe reader or equivalent. Please **do NOT substitute** any other document (text file, scanned image, etc.).

Article title : Integrated model of the left ventricle for the analysis of regional

Human and animal rights

☐ The authors declare that the work described has been carried out in accordance with the Declaration of Helsinki of the World Medical Association revised in 2013 for experiments involving humans as well as in accordance with the EU Directive 2010/63/EU for animal experiments.

☑ The authors declare that the work described has not involved experimentation on humans or animals.

Informed consent and patient details

☐ The authors declare that this report does not contain any personal information that could lead to the identification of the patient(s) and/or volunteers.

☐ The authors declare that they obtained a written informed consent from the patients and/or volunteers included in the article and that this report does not contain any personal information that could lead to their identification.

☐ The authors declare that the work described does not involve patients or volunteers.

Disclosure of interest

☑ The authors declare that they have no known competing financial or personal relationships that could be viewed as influencing the work reported in this paper.

☐ The authors declare the following financial or personal relationships that could be viewed as influencing the work reported in this paper:

Funding

☐ This work did not receive any grant from funding agencies in the public, commercial, or not-for-profit sectors.

☑ This work has been supported by:

French National Research Agency (ANR) (ANR-16-CE19-0008-01) (project MAESTRo)

Author contributions

☐ All authors attest that they meet the current International Committee of Medical Journal Editors (ICMJE) criteria for Authorship.

☑ All authors attest that they meet the current International Committee of Medical Journal Editors (ICMJE) criteria for Authorship. Individual author contributions are as follows:

O. Duport: Formal analysis, Data curation, Methodology, Software, Writing - review & editing.
V. Le Rolle: Conceptualization, Funding acquisition, Data curation, formal analysis, Methodology, Software, Supervision,Writing - Original draft,Writing - review&editing.
E. Galli: Data curation, Supervision,Writing - review&editing.
D. Danan: formal analysis, Methodology, Software, Writing - review & editing.
E. Darrigrand: Formal analysis, Methodology, Writing - review&editing.
E. Donal: Data curation,Writing - Original draft preparation, Supervision,Writing - review & editing.
A. I. Hernández: Conceptualization, Data curation, formal analysis, Methodology, Software, Writing

CRediT authorship contribution statement

O. Duport: Formal analysis, Data curation, Methodology, Software, Writing - review & editing. **V. Le Rolle:** Conceptualization, Funding acquisition, Data curation, formal analysis, Methodology, Software, Supervision, Writing - Original draft, Writing - review & editing. **E. Galli:** Data curation, Supervision, Writing - review & editing. **D. Danan:** formal analysis, Methodology, Software, Writing - review & editing. **E. Darrigrand:** Formal analysis, Methodology, Writing - review & editing. **E. Donal:** Data curation, Writing - Original draft preparation, Supervision, Writing - review & editing. **A.I. Hernández:** Conceptualization, Data curation, formal analysis, Methodology, Software, Writing - original draft, Supervision, Writing - review & editing.